Journal of Minerals and Materials Characterization and Engineering, 2022, 10, 225-241
https://www.scirp.org/journal/jmmce
ISSN Online: 2327-4085
ISSN Print: 2327-4077

Electrochemical Corrosion Study in H_2SO_4 of NiAl with Cu Additions, Microstructure and Micro-Hardness at Room Temperature

Jesús M. Colín de la Cruz[1*], Sergio A. Serna Barquera[2], Alvaro Torres-Islas[1], Arturo Molina-Ocampo[2], Edgar Valenzuela[3], José G. González Rodríguez[2]

[1]Universidad Autónoma del Estado de Morelos, Facultad de Ciencias Químicas e Ingeniería, UAEM-FCQeI. Av. Universidad 1001Colonia Chamilpa, Cuernavaca Morelos, México
[2]Universidad Autónoma del Estado de Morelos Centro de Investigación en Ingeniería y Ciencias Aplicadas, UAEM-CIICAp, Cuernavaca Morelos, México
[3]UABC, Baja California Sur, México
Email: *jcolin@uaem.mx

How to cite this paper: de la Cruz, J.M.C., Barquera, S.A.S., Torres-Islas, A., Molina-Ocampo, A., Valenzuela, E. and Rodríguez, J.G.G. (2022) Electrochemical Corrosion Study in H_2SO_4 of NiAl with Cu Additions, Microstructure and Micro-Hardness at Room Temperature. *Journal of Minerals and Materials Characterization and Engineering*, **10**, 225-241.
https://doi.org/10.4236/jmmce.2022.103018

Received: March 9, 2022
Accepted: April 19, 2022
Published: April 22, 2022

Abstract

For many years, intermetallic materials promise applications in a wide variety of technology areas. NiAl intermetallic compound is material that exhibits important characteristics such as high corrosion resistance and low density besides its ability to retain strength and stiffness at elevated temperatures. However NiAl intermetallic is too hard, brittle and exhibits very low ductility at room temperature being the reason because this material is not yet available for structural applications. In order to increase the ductility of the NiAl intermetallic compound, the addition of a third alloying element has been proved, nevertheless it is important to determine if such additions decrease or increase the hardness and the corrosion resistance of the alloy. So, the present investigation reports the corrosion performance of the NiAl intermetallic compound modified with Cu, emphasizing the EIS analysis and the relation between physical parameters and the modelling equations used in the Equivalent Electric Circuit. It was found that the addition of Cu promotes the formation of the γ'-Ni_3Al phase in Cu contents greater than 15 at. %, in addition to a decrease in micro hardness and an increment in the I_{corr} values. In this way, the electrochemical characterization evidenced a high corrosion resistance of these intermetallic alloys.

Keywords

NiAl-Cu, Corrosion Behavior, Electrochemical Impedance Spectrum, Vickers Micro Hardness, Microstructure

1. Introduction

Intermetallic compounds in their simplest conception are the result of the combination of two or more metallic elements in well-defined stoichiometric proportions [1] [2] [3] and [4]. The resulting alloy has specific properties, including high mechanical resistance, high melting point, and high resistance to corrosion and oxidation [1] [2], which is why they have been widely studied [4] [5]. Particularly the nickel and aluminum containing alloys have aroused great interest because they are widely used in high temperature and excessive corrosion environments such as heat exchangers [5] [6] [7] and [8]. Several intermetallic compounds can be formed in the Ni-Al system but one of the most interesting is the NiAl intermetallic which melts at 1638˚C and exhibits great chemical stability at room temperature [1]. Despite the above, intermetallic compounds are very hard and brittle at room temperature, so the addition of alloying elements has been explored in order to make them more ductile [9] [10]. In a previous study it was found that Cu and Fe additions can increase the ductility of the NiAl intermetallic [9] [10], however it is necessary to determine if these additions affect the corrosion resistance of the alloy.

In early 1980s Mansfield and Lorenz showed the wide possible range of application of electrochemical impedance spectroscopy (EIS) with respect to corrosion processes [11] [12] [13]

Electrochemical impedance is the opposition of an electrochemical system to the alternating current that flows through it. If harmonic AC voltage of small amplitude is applied to the system, the response of the electrode/electrolyte interphase will produce a resistive-capacitive behavior, causing a lead in the flow of the sinusoidal current with respect to the supplied voltage. One of the main tools used in impedance study is to establish an equivalent electric circuit, fitting the response of the system under study [14] [15] [16]

Such electric circuits are typically modeled as a series and parallel resistance (R) and capacitance (C) arrangements. Active resistance reflects the influence of electrolyte electrical resistance, slowness of charge transfer through the electrode/solution interface and/or of diffusion of electrochemically active substances. While capacitive impedance is related to the charge accumulation in the double electrical layer, diffusion of the surfactants presented in a solution and their adsorption (desorption) on an electrode [17] [18].

Between the huge numbers of reports on EIS application to various corrosion systems, this paper present the results continuing past publications of electrochemical results [19] emphasizing the study of the intermetallic corrosion response and the relation between its physical parameters with the electrical elements of the Equivalent Electric Circuit (EEC).

Four as-cast specimens were prepared and characterized using X-ray diffraction, scanning electron microscopy and Vickers Microhardness. Biphasic microstructures composed of the B2 β-Ni(Al,Cu) and $L1_2$ γ'-$(Ni,Cu)_3Al$ phases were observed in three of the four alloys, and only B2 β-Ni(Al,Cu) in the other one.

The electrochemical characterization evidenced a high corrosion resistance compared to similar alloys, related to the formation of a protective layer that grows proportionally to the aluminum content in the sample.

2. Experimental Procedures

Four NiAl intermetallic alloys with Cu additions (Cu as macro alloying element) were prepared by melting mixtures of Al (99.98%), electrolytic Cu (99.98%) and Ni (99.98%), in a Leybold–Heraeus Mod. HV-264 vacuum induction furnace under an Ar atmosphere, using a graphite crucible. Alloys were prepared according the compositions listed in Table inserted in Figure 1 at 1700˚C and then cast it into iron ingot molds producing blocky ingots of about 150 g in weight and left cooled at room temperature. The calculation of the alloy element proportions was performed according to the equilibrium phase diagram illustrated in Figure 1.

The obtained ingots were identified and sectioned to test it and perform its mechanical, microstructural and electrochemical characterization. A Jeol JSM 6400 scanning electron microscope was used for microstructural characterization of the intermetallic ingots. X-ray diffraction analysis was used to identify the present phases in the samples, and it was performed on a SIEMMENS D-5000, employing Cu radiation and a Fe filter. Micro hardness Vickers tests (0.025) were carried out in a Bhueler MHT2 Micro hardness tester.

Electrochemical Characterization

The electrochemical behavior in acid media of four intermetallic Ni-Al-Cu samples with different Al/Cu proportions was determined. The experiments were performed in a 3 electrodes cell with a Biologic SP 300 Potentiostat/Galvanostat in H_2SO_4 0.5 M at 25˚C, using a Pt mesh as counter electrode, while all potentials were measured and referred to a saturated Calomel electrode.

The 1 cm^2 Ni-Al-Cu samples were encapsulated in epoxy resin and polished with 600, 800 and 1000 grit silicon carbide paper, then with a 0.3 μm alumina

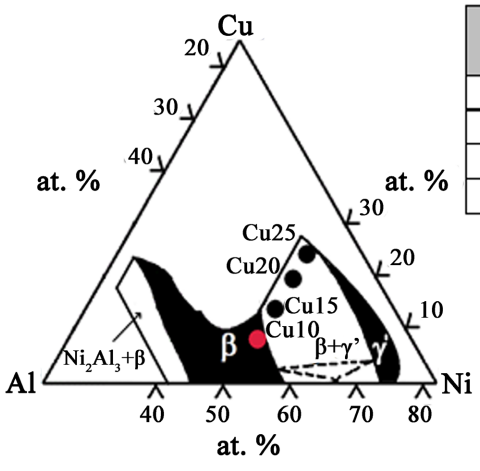

Sample	Composition at. %		
	Al	Cu	Ni
Cu10	40	10	Bal
Cu15	35	15	Bal
Cu20	30	20	Bal
Cu25	25	25	Bal

Figure 1. Ternary phase diagram of the Ni-Al-Cu system, ref. [20]

suspension in a felt cloth. The polished electrodes were cleaned with acetone in ultrasonic bath and rinsed with deionized water prior any electrochemical evaluation. For each evaluation, the solution was de-aerated by bubbling N_2 for 20 minutes, and the open circuit potential was measured to ensure a variation lower than 5 mV/min. After open circuit potential stabilization, the electrochemical performance of the Ni-Al-Cu intermetallic electrodes was evaluated by EIS. An AC 10 mV perturbation was applied, varying the signal frequency from 200 kHz to 10 mHz while the potentiodynamic polarization evaluation was conducted from +1500 mv to −400 mV vs open circuit potential, at a scan rate of 1 mV/s.

3. Results and Discussion

3.1. Microstructure

According to the compositions shown in the composition table and the ternary Ni-Cu-Al phase diagram [20] of **Figure 1**, the Cu10 alloy lies into the β-Ni(Al,Cu) monophasic field while the Cu15, Cu20 and Cu25 alloys lies into the biphasic field formed by the β-Ni(Al,Cu) + γ'-$(Ni,Cu)_3Al$ phases. However, Cu15 is closer to the β-Ni(Al,Cu) monophasic field which suggest that the presence of such phase is higher than γ'-$(Ni,Cu)_3Al$ phase and this is confirmed by x-ray pattern showed in **Figure 2(b)**.

In the same way, the X-Ray diffraction patterns confirm that the microstructures of Cu15, Cu20 and Cu25 alloys are biphasic but with morphological differences as described next. **Figure 2(b)** shows that Cu15 alloy is formed by dendrites of the cubic β-Ni(Al,Cu) phase surrounded by a like eutectic microconstituent composed by the β-Ni(Al,Cu) + γ'-$(Ni,Cu)_3Al$ phases in the interdendritic spaces. On the other hand, in **Figure 2(c)** it can be seen that the microstructure of Cu20 alloy is composed by like flakes of γ'-$(Ni,Cu)_3Al$ immersed into a matrix of β-Ni(Al,Cu) + γ'-$(Ni,Cu)_3Al$ phases. Meanwhile the microstructure of the Cu25 alloy is composed by the same β-Ni(Al,Cu) + γ'-$(Ni,Cu)_3Al$ phases but as biphasic dendrites immersed into a presumably γ'-$(Ni,Cu)_3Al$ phase. It is important to mention that γ'-$(Ni,Cu)_3Al$ phase showed two different crystal structures, one of them cubic indicated in the x-ray patterns as γ'_C and the other one tetragonal indicated in the x-ray patterns as γ'_T.

3.2. Microhardness Vickers

Six Vickers microhardness test indentations were made for each sample in different zones, using 50 g as load test. The results shown in **Figure 3** correspond to the average of such readings as a function of the copper content in the alloy. It can be observed that copper additions produce a tendency to decrease the hardness of the alloys starting with the one with 10 at. % Copper which exhibits 354 HV value and ending with that of 25 at. % Copper which exhibits 327 HV value, such difference represents less than 8% decrease. The decrease presumably is due to the transition and disappearance of the β-(Ni,Cu)Al phase in the Cu10 and Cu15 samples, see the first box in **Figure 3**, to the rising of the γ'-$(Ni,Cu)_3Al$ phase

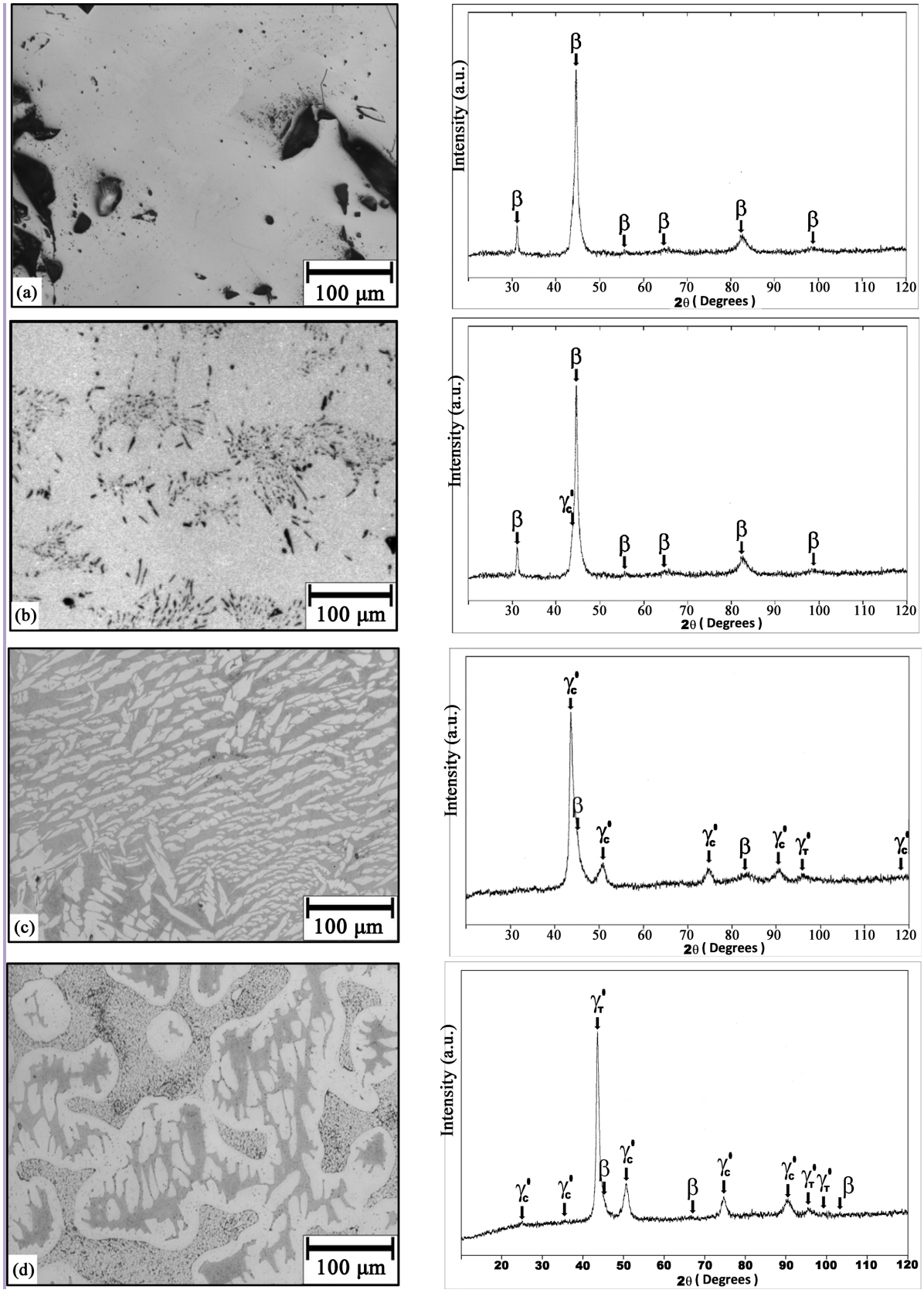

Figure 2. Microstructures observed in the alloys under study and its corresponding X-Ray diffraction patterns. (a) Cu10; (b) Cu15; (c) Cu20 and (d) Cu25.

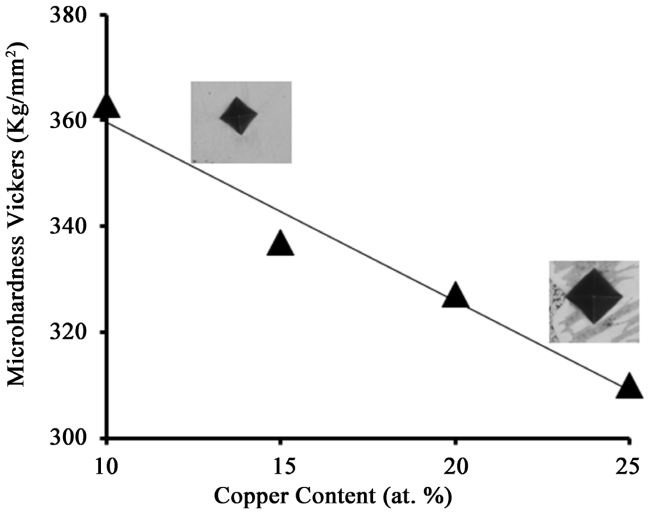

Figure 3. Vickers microhardness values registered in the intermetallic alloys modified with copper. The first box micrograph is a representative indentation observed in the Cu5 and Cu10 samples. The second one corresponds to the observed in the Cu15 and Cu20 samples

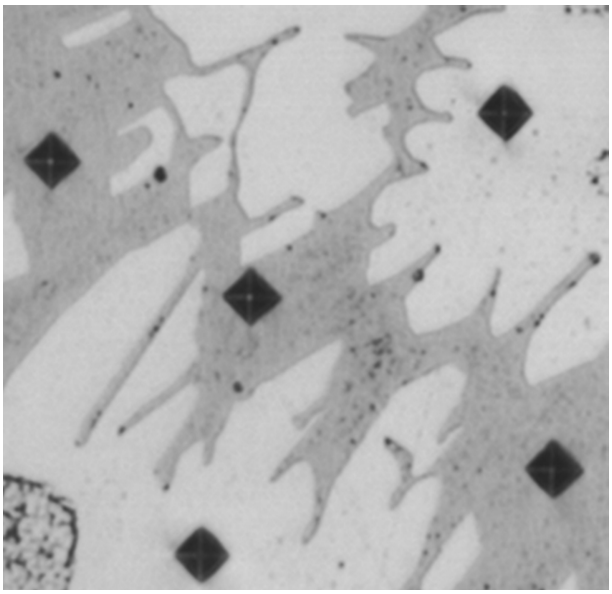

Figure 4. Vickers microhardness indentations impressed in the cubic γ_C'-$(Ni,Cu)_3Al$ and tetragonal γ_T'-$(Ni,Cu)_3Al$ phases present in the Cu25 sample surface with the same 50 g load test. The similar size suggests that there is no big difference between Vickers Microhardness values.

in the Cu15 and Cu 20 samples, see the second box, according to the X-ray patterns showed in the **Figure 2**. There was not observed a big microhardness difference between the cubic γ_C'-$(Ni,Cu)_3Al$ and tetragonal γ_T'-$(Ni,Cu)_3Al$ phase as it can be seen in **Figure 4**, which shows the indentations with almost the same size.

3.3. Electrochemical Characterization of Intermetallic Electrodes

Four Ni-Cu-Al intermetallic samples were electrochemically evaluated and its

corrosion behavior in H_2SO_4 0.5 M determined. The test included the open circuit potentials measurement, EIS analysis and potentiodynamic polarization. All experimental data are shown in doted lines and for simplicity, only in the Nyquist diagrams, the solid lines representing the simulation results are included.

The open circuit potentials for each Ni-Cu-Al intermetallic electrode are presented in Figure 4. The measured values exhibited a mix potential highlighting the composition and quantity of the materials involved in the alloy, where a relation between the Al content and a shift to most electronegative potentials is observed. While the Cu rich samples evidenced a steadier potential, with faster stabilization than those with a higher Al/Cu proportion.

The polarization curves are shown in Figure 5. The results agree with the open circuit measurements, where the increment in the Cu content in the samples displaces the potential (E_{corr}) to more positive values. Conversely, it was found that samples with higher Al content exhibited lower corrosion currents, as can be seen in Table 1. Polarization curves display an active-passive behavior, exhibiting 2 passive zones with some current fluctuations. For potential values

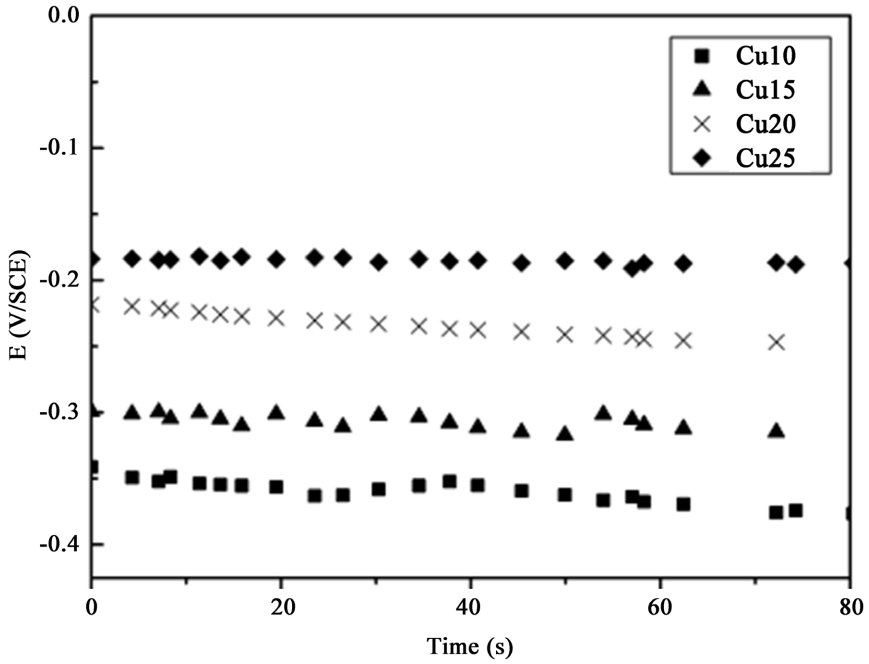

Figure 5. Open circuit potentials in H_2SO_4 0.5 M for the Ni-Cu-Al intermetallic samples with different Al/Cu proportions.

Table 1. Corrosion potential and current densities of the intermetallic alloys.

Alloy	E_{corr} (V)	i_{corr} (mA·cm^{-2})
Cu10	−0.432 ± 0.002	4.86 ± 0.6
Cu15	−0.422 ± 0.005	1.01 ± 0.3
Cu20	−0.417 ± 0.008	12.48 ± 0.4
Cu25	−0.146 ± 0.007	120 ± 0.7

between −300 and −100 mv, passive zone is mainly to the formation of an Al_2O_3 oxide layer which protects the alloy.

The presence of Cu in the alloy makes possible the formation of both CuO and Cu_2O oxides which are incorporated and competes with the Al_2O_3 layer during its formation, leaving to an unstable passive layer which is dissolved in some places where it is not completely formed, giving place to the current fluctuations. As the Cu contents increases, these fluctuations increase in frequency and current intensity due to the fact that more copper oxides compete with the Al_2O_3. Once the first passive zone is formed and it is broken down, anodic dissolution of this layer gives rise to the transpassive region and to a second passive zone, at potentials more anodic than 0 mV, which might be due to the presence of CuO and Cu_2O oxides, less protective than Al_2O_3.

3.4. Electrochemical Impedance Spectroscopy

After a stable open potential was achieved, the electrochemical impedance response was determined at open circuit conditions. The Nyquist diagrams of Figure 6 show the impedance behavior for the intermetallic samples with an inset that displays the details of the response for the Cu25 and Cu20 Samples. Nyquist diagrams displays a single depressed, capacitive semicircle with its center at the real axis, indicating a charge transfer controlled corrosion mechanism. As the Cu contents increase, the semicircle diameter decreases.

When analyzing the Nyquist diagrams of Figure 6, it can be seen that all samples exhibit a main low frequencies semicircle that increases its diameter with the increment of Al content in the sample, normally attributed to the formation of a protective layer on the metallic surface. Whereas at high frequencies, only a small semicircle is observed in the higher Al content alloys such as Cu10 and Cu15, and its attributed to the charge exchange between the passive layer and the

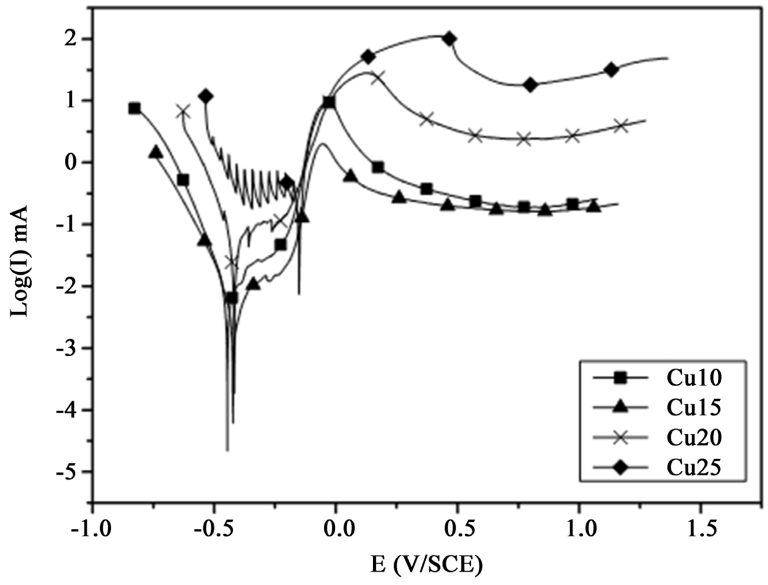

Figure 6. Polarization curves of Ni-Cu-Al electrodes in H_2SO_4 0.5 M.

bulk material and can be better identified in the phase angle diagrams of Figure 7 [21] with the presence of two peaks, whereas Cu20 and Cu25 alloys exhibited one peak only, indicating the absence of such a passive layer or a passive layer not-protective enough.

The phase angle diagrams in Figure 8 shows the presence of two peaks, or two

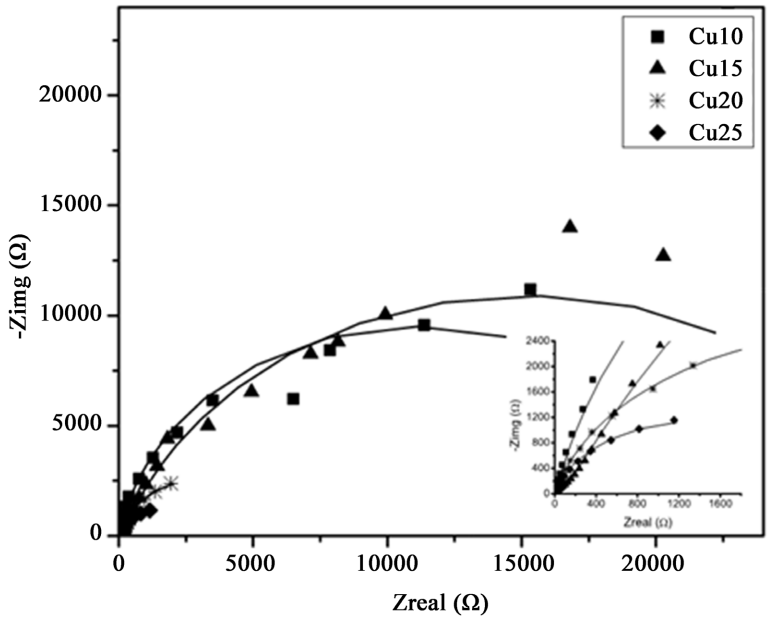

Figure 7. The Nyquist plot for the intermetallic electrodes. The EIS results of Cu20 and Cu25 are shown in an amplified scale in the inset.

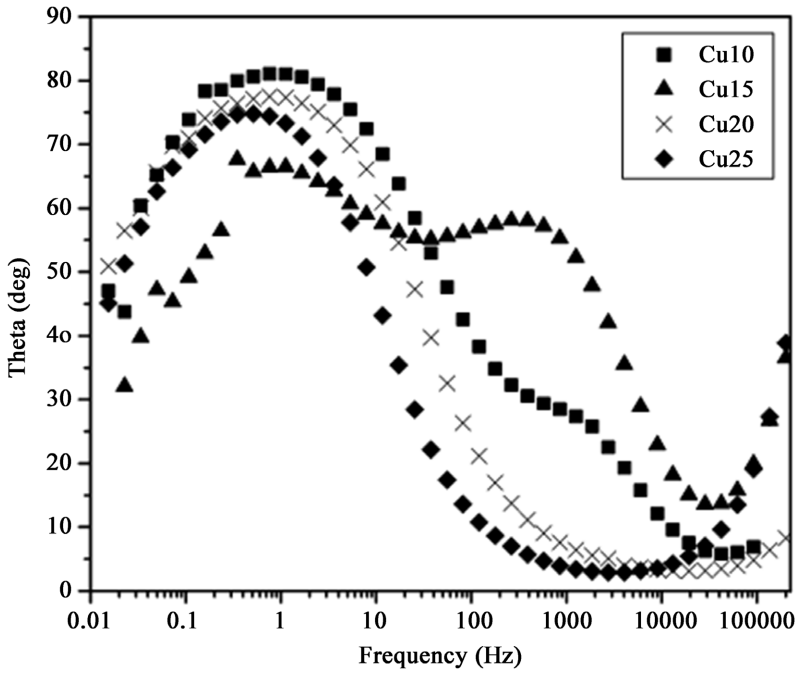

Figure 8. The phase diagrams exhibit a single time constant for the Cu25, Cu20 samples with low Al content and an additional peak at high frequencies only for the Cu10 and Cu15 with high Al.

constant phase elements, for alloys containing either 10% or 15% Cu, whereas for copper contents of either 20 or 25, the presence of two peaks was not so evident, only one peak can be observed, and, thus, only one constant phase element. When analyzing the low frequencies response of the phase angle plots, a highly capacitive behavior near the 800 Hz is observed in all samples, with phase angles from 75˚ for the Cu25 sample, up to 81˚ in the Cu10 electrode. This low frequency peak is related to the outer passive layer response, and in agreement with the Nyquist plots, the capacitive contribution increases with the Al content. Similar behavior has been reported elsewhere [22] [23] [24] [25] and attributed to the thickening of the protective layer with a consequent increase in the Charge Transfer Resistance, as observed in the impedance magnitude plots of **Figure 8**.

It is a common practice to simulate electrochemical impedance spectroscopy data by using equivalent electric circuits. The electrochemical impedance response was well adjusted using the Electrical Equivalent Circuit (EEC) as that shown in **Figure 9**, by using electric resistances and capacitances. Due to the fact that observed semicircles are depressed due to metal dissolution, ideal capacitances are replaced by Constant Phase Elements (CPE to simulate the capacitive behavior due to semicircle depressions related to surface electrode inhomogeneity [26] [27]. In **Figure 10**, the electrolyte or solution resistance is represented by Rs, the corrosion products layer resistance is represented by R_1 whereas the constant phase element associated to this film capacitance is represented by CPE_1 and both are associated to the electrochemical reactions taking place at the metal/corrosion product film interface. The double electrochemical layer resistance is represented by R_2 which represents the charge transfer resistance, R_{ct}, whereas the constant phase element associated to this double electrochemical layer is

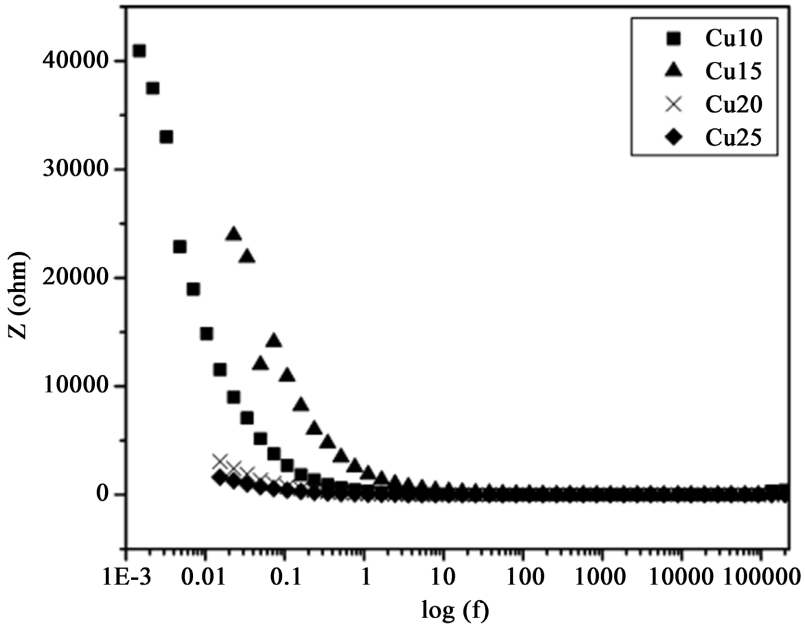

Figure 9. Absolute impedance ([Z]) impedance modulus |Z|.

represented by CPE_2 or CPE_{dl}. When evaluating the corrosion resistance performance of metallic alloys in Nyquist plots, the semicircle located at medium and low frequencies is normally attributed to the interactions between the outer protective layer and the electrolyte and its represented in the EEC by the R_2CPE_2 couple; On the other hand, the inner high frequencies response related to the charge transference between the passive layer and the bulk is simulated with the R_1CPE_1 branch and the sum of both diameters is correlated to the total material corrosion resistance (R_{CT}). [28] [29]

The relation between the capacitive behavior and the protective layer reinforcement can be explained if considering the following relations, that describe the capacitor and capacitive reactance, along with the impedance and theta values for an RC parallel arrangement (Equations (1)-(5)).

$$C_{dl} = E\frac{A}{L} \tag{1}$$

$$X_{Cdl} = \frac{-j}{2\pi fC_{dl}} \tag{2}$$

$$Z_{Total} = \frac{RX_{Cdl}^2 - jR^2X_{Cdl}}{R^2 + X_{Cdl}^2} \tag{3}$$

$$Z_{Real} = \frac{RX_{Cdl}^2}{R^2 + X_{Cdl}^2} \tag{4}$$

$$Theta = \arctan\frac{Z_{Img}}{Z_{Real}} \tag{5}$$

Equation (1) represents the capacitance value, where E is the permittivity of the dielectric, in this case the passive layer, A the effective surface of the electrode and L the distance between electrical charges separated by the same protective layer. As it can be seen in the Nyquist and the absolute impedance modulus plots, the more Al content in the samples, lead to a higher corrosion resistance, presumably due the aluminum oxide passive layer thickening, that increase the L value in Equation (1). If this were the case and assuming a constant effective electrode surface, according with the same equation, that change in the material surface will lead to a decrement of the outer capacitance (represented as CPE_2) and an increase in the R_2, as can be verified in the values presented in Table 2. This table shows that the corrosion resistance of the alloys is given by the

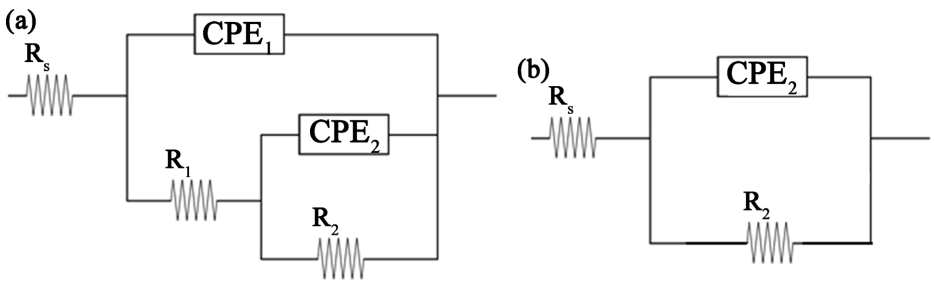

Figure 10. The Electrical Equivalent Circuit used to fit the impedance data for alloys containing (a) 10 and 15, and (b) 20 and 25 Cu.

Table 2. Experimental results obtained from the electrochemistry tests performed in the intermetallic alloys.

Sample	R_S (Ω)	CPE_1 (mF/cm^2)	n_1	R_1 (Ω)	CPE_2 (mF/cm^2)	n_2	R_2 (Ω)
Cu10	2.67	0.17	0.84	8.84	0.35	0.93	22,374
Cu15	5.94	724	0.79	365	834	0.94	29,736
Cu20	3.55	1.65	0.83	---	1.04	0.80	6328
Cu25	5.04	0.80	1.00	---	4.11	0.85	2775

resistance of the corrosion product layer, R_1, since they are much higher than that for the electrochemical layer, R_2. We can see that the value for the corrosion products film, R_2, is much higher for alloys containing 10 and 15 Cu than that for alloys containing 20 and 25 Cu, indicating a superior corrosion resistance which decreases with the Cu contents. The n2 value for alloys containing either 10 or 15 Cu was close to 1.0 due to a lower surface roughness because ot their higher corrosion resistance.

In this way, when considering the relations in Equations (1) and (2) and the impedance of the EEC in Equations (3) and (4), the decrease in the Cdl will increment the capacitive reactance (X_{Cdl} in Equation (2)), causing an increase of the real component of the total impedance of Equation (3) and better appreciated in Equation (4).

Under this condition, the Zimg/Zreal relation and hence its phase angle theta (Equation (5)) has to decrease, being particularly evident in the low frequencies range of **Figure 7**, where the impedance is maximum but theta minimum, due the largest contribution of the Zreal impedance. Furthermore, when following the behavior of phase angle in **Figure 7**, it can be seen that when frequency increase the opposite response is observed, due that larger frequencies will drop again the X_{Cdl} values (Equation (2)) and consequently the Zreal component, increasing the value of the phase angle theta in the high Al content samples, as it can be seen in **Figure 8** and verified in a number of documents, that show how the thickening of the passive layer, is associated to a displacement in the peak of the phase angle into higher frequencies believably because the above discussed process [24] [30] [31] [32] [33].

4. Discussion

According to the results reported above, there are two mainly events. The one is that, the augmentation of Cu content in the alloy induces the disappearance of the β-(Ni,Cu)Al phase and the raising of the γ'-$(Ni,Cu)_3Al$ phase observing a decrement in the microhardness Vickers values. The second one is that, as the of Cu increases, the corrosion resistance of the material also increases, attributable to the thickening of the passive layer. Such results suggest that Cu additions induce a phase transformation from β-(Ni,Cu)Al phase to the γ'-$(Ni,Cu)_3Al$ which is less hard and less resistant to the corrosion process as it can be seen in **Figure 11**.

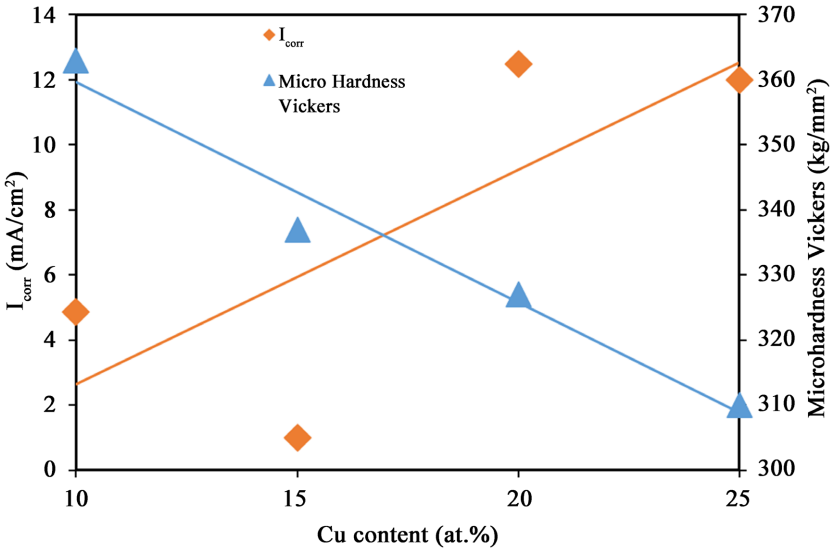

Figure 11. *Icorr* and microhardness Vickers as a function of the Cu content in the alloy.

For passivation to occur, it is necessary the formation of a protective film which must be adherent, without porous and, chemically inert in the solution. It is well known that, if the formed film on the alloy is flaws-free, the underlying alloy will not denote severe corrosion, and no pitting, but if the film contains defects or any other discontinuities, the alloy will suffer from corrosion. Pitting arises at the dissolution of the metal within defects in the film surface when the bare metal is unprotected to the aggressive anions in the electrolyte.

The locations of or localized corrosion stand linked to the metal surface conditions, such as microstructure, surface preparation, and to the composition of the electrolyte. To develop pitting, anions (Cl^-, SO_4^-, Br^-, I^-, etc.) must first adsorb on the surface of films. With the presence of such anions, pitting occurs with competition of the repair process of the passive film by the active dissolution of the intermetallic alloys defects. The presence of second phases or the establishment of micro cells, where one of the phases has either different chemical composition or microstructure, one of these phases will act as cathode and the other as an active anode. This will cause the preferential dissolution of one of the phases, the one which acts as active anode, inducing preferential, localized dissolution within the alloy. To avoid the pitting, the film must stop the adsorption of anions and interrupt the breakdown of passivity. The intermetallic alloys that contain Al, form an alumina (AlO_2) layer that protect them against corrosion. O the other hand the effect of Cu is to promote the presence of second phases within the intermetallic alloy, inducing the formation of micro galvanic cells, and, thus, the preferential dissolution of one of the phase. The phase with less corrosion resistance, will act as an anode.

As be expected the high Ni content is always useful, however, there is a critical Ni contents within the corrosion products over which the increase of the Ni contents reduces the corrosion resistance [8] [9] [10]. The decrease in *Icorr* can remain understood by the dissolution of Ni with the creation of Ni^{2+} and subse-

quent d the formation of a barrier of $Ni(OH)_2$ or NiO [11].

5. Conclusions

The corrosion resistance of the NiAl intermetallic alloy microalloyed with 10, 15, 20 and 25 at %. Cu in a 0.5M H_2SO_4 solution has been studied. Biphasic microstructures composed of the B2 β-Ni(Al,Cu) and $L1_2$ γ'-$(Ni,Cu)_3Al$ phases were observed in all cases. It was observed that Cu additions to the NiAl intermetallic alloy produce the tendency of disappearance of the β-(Ni,Cu)Al phase and the raising of the γ'-$(Ni,Cu)_3Al$ phase, which is according to the Ni-Al-Cu ternary phase diagram alloy. In the same way, the microstructure changes from monophasic β-(Ni,Cu)Al phase to a dendritic and like flakes microstructures are composed by the β-(Ni,Cu)Al and γ'-$(Ni,Cu)_3Al$ phases observing a decrement in the microhardnes Vickers and an increment in the *Icorr* values. In this way, the electrochemical characterization evidenced a high corrosion resistance of these intermetallics.

It can be seen that Cu additions to the NiAl alloy made the *Ecorr* value of the NiAl to move towards more noble values however, the NiAl intermetallic alloys exhibited a preferential, localized kind of corrosion, which was caused by the establishment of micro galvanic cells, which is resulted by the formation of second phases within the alloy. Compared with the unalloyed NiAl alloy, additions of Cu up to 15% did not affect the passive current density, Ipass. The lowest Ipass value was obtained with 20% Cu, whereas the highest values were obtained with 25% Cu. In all cases, additions of Cu to the NiAl intermetallic decreased the Epit value. These results were discussed in terms of the incorporation of second phase particles in to the intermetallic passive layer modifying its electrochemical properties.

Conflicts of Interest

The authors declare no conflicts of interest regarding the publication of this paper.

References

[1] Darolia, R. (1991) NiAl Alloys for High-Temperature Structural Applications. *JOM*, **43**, 44-49. https://doi.org/10.1007/BF03220163

[2] Busso, E.P. and Mcclintock, F.A. (1994) Mechanisms of Cyclic Deformation of NiAl Single Crystals at High Temperatures. *Acta Metallurgica et Materialia*, **42**, 3263-3275. https://doi.org/10.1016/0956-7151(94)90459-6

[3] Jayaram, R. and Miller, M.K. (1994) An Atom Probe Study of Grain Boundary and Matrix Chemistry in Microalloyed NiAl. *Acta Metallurgica et Materialia*, **42**, 1561-1572. https://doi.org/10.1016/0956-7151(94)90366-2

[4] Field, R. D., Lahrman, D.F. and Darolia, R. (1991) Slip Systems in 〈001〉 Oriented NiAl Single Crystals. *Acta Metallurgica et Materialia*, **39**, 2951-2959. https://doi.org/10.1016/0956-7151(91)90027-X

[5] Jafari, R. and Sadeghi, E. (2019) High-Temperature Corrosion Performance of

HVAF-Sprayed NiCr, NiAl, and NiCrAlY Coatings with Alkali Sulfate/Chloride Exposed to Ambient Air. *Corrosion Science,* **160**, Article ID: 108066. https://doi.org/10.1016/j.corsci.2019.06.021

[6] Abu-Warda, N., López, A.J., López, M.D. and Utrilla, M.V. (2019) High Temperature Corrosion and Wear Behavior of HVOF-Sprayed Coating of Al_2O_3-NiAl on AISI 304 Stainless Steel. *Surface and Coatings Technology*, **359**, 35-46. https://doi.org/10.1016/j.surfcoat.2018.12.047

[7] Liu, Y.D., Sun, J., Pei, Z.L., Li, W., Liu, J.H., Gong, J. and Sun, C. (2020) Oxidation and Hot Corrosion Behavior of NiCrAlYSi+NiAl/cBN Abrasive Coating. *Corrosion Science*, **167**, Article ID: 108486. https://doi.org/10.1016/j.corsci.2020.108486

[8] Yang, Y.F., Liu, Z.L., Ren, P., Wang, Q.W., Bao, Z.B., Zhu, S.L. and Li, W. (2020) Hot Corrosion Behavior of Pt+Hf Co-Modified NiAl Coating in the Mixed Salt of Na_2SO_4-NaCl at 900 ˚C. *Corrosion Science*, **167**, Article ID: 108527. https://doi.org/10.1016/j.corsci.2020.108527

[9] Colin, J., Gonzalez, C., Herrera, R. and Juarez-Islas, J.A. (2002) Analysis of Chill-Cast NiAl Intermetallic Compound with Copper Additions. *Journal of Materials Engineering and Performance*, **11**, 487-491. https://doi.org/10.1361/105994902770343700

[10] Colín, J., Serna, S., Campillo, B., Flores, O. and Juárez-Islas, J. (2008) Microstructural and Lattice Parameter Study of As-Cast and Rapidly Solidified NiAl Intermetallic Alloys with Cu Additions. *Intermetallics*, **16**, 847-853. https://doi.org/10.1016/j.intermet.2008.03.001

[11] Lorenz, W.J. and Mansfield, F. (1981) Determination of Corrosion Rates by Electrochemical DC and AC Methods, *Corrosion Science*, **21**, 647-672. https://doi.org/10.1016/0010-938X(81)90015-9

[12] Aksut, A.A., Lorenz, W.J. and Mansfield, F. (1982) The Determination of Corrosion Rates by Electrochemical D.C and A.C Methods—II. Systems with Discontinuous Steady State Polarization Behavior. *Corrosion Science*, **22**, 611-619. https://doi.org/10.1016/0010-938X(82)90042-7

[13] Mansfeld, F. (1990) Electrochemical Impedance Spectroscopy (EIS) as a New Tool for Investigating Methods of Corrosion Protection. *Electrochemica Acta*, **35**, 1533-1544. https://doi.org/10.1016/0013-4686(90)80007-B

[14] Juettner, K., Lorenz, W. J., Kendig, M.W. and Mansfeld, F. (1988) Electrochemical Impedance Spectroscopy on 3-D Inhomogeneous Surfaces. *Journal of the Electrochemical Society*, **135**, 332-339. https://doi.org/10.1149/1.2095610

[15] Scully, J.R., Silverman, D.C. and Kendig, M.W. (Eds.) (1991) Electrochemical Impedance: Analysis and Interpretation. ASTM Special Technical Publication No. 1188, ASTM International, Philadelphia, 37.

[16] Fletcher, S. (1994) Tables of Degenerate Electrical Networks for Use in the Equivalent-Circuit Analysis of Electrochemical Systems. *Journal of the Electrochemical Society*, **141**, 1823-1826. https://doi.org/10.1149/1.2055011

[17] Randles, E.B. (1947) Kinetics of Rapid Electrode Reactions. *Discussions of the Faraday Society*, **1**, 11-19. https://doi.org/10.1039/df9470100011

[18] Macdonald, D.D. (2006) Reflections on the History of Electrochemical Impedance Spectroscopy. *Electrochimica Acta*, **51**, 1376-1388. https://doi.org/10.1016/j.electacta.2005.02.107

[19] González-Rodriguez, J.G., Colín, J.C., Serna, S., Campillo, B. and Albarran, J.L. (2007) Effect of Macroalloying with Cu on the Corrosion Resistance of Rapidly So-

lidified NiAl Intermetallic in 0.5M H_2SO_4. *Materials Science and Engineering*: *A*, **448**, 158-164. https://doi.org/10.1016/j.msea.2006.11.079

[20] Bradley, A.J. and Lipson, H. (1938) An X-Ray Investigation of Slowly Cooled Copper-Nickel-Aluminium Alloys. *Proceedings of the Royal Society of London*, *Series A*, **167**, 421-438. https://doi.org/10.1098/rspa.1938.0139

[21] Niu, Q., Li, Z., Cui, G. and Wang, B. (2017) Effect of Flow Rate on the Corrosion Behavior of N80 Steel in Simulated Oil Field Environment Containing CO_2 and HAc. *International Journal of Electrochemical Science*, **12**, 10279-10290. https://doi.org/10.20964/2017.11.23

[22] Osórioa, W.R., Freitas, E.S. and Garcia, A. (2013) EIS and Potentiodynamic Polarization Studies on Immiscible Monotectic Al–In Alloys. *Electrochim. Acta*, **102**, 436-445. https://doi.org/10.1016/j.electacta.2013.04.047

[23] Laboulais, J.N., Mata, A.A., Borrás, V.A. and Muñoz, A.I. (2017) Electrochemical Characterization and Passivation Behaviour of New Beta-Titanium Alloys (Ti35Nb10Ta-XFe). *Electrochimica Acta*, **227**, 410-418. https://doi.org/10.1016/j.electacta.2016.12.125

[24] Díaz, E.F., Serna, S., Porcayo-Calderon, J., Cuevas, C., Torres-Islas, A., Molina, A. and Colin, J. (2013) Corrosion Performance of a Novel NiAl-Cu Intermetallic HVOF Protective Coating Part I: Low Temperature Corrosion in 0.5 M H_2SO_4. *International Journal of Electrochemical Science*, **8**, 7156-7174

[25] Sherif, E.M., El-Danaf, E.A., Soliman, M.S. and Almajid, A.A. (2012) Corrosion Passivation in Natural Seawater of Aluminum Alloy 1050 Processed by Equal-Channel-Angular-Press. *International Journal of Electrochemical Science*, **7**, 2846-2859.

[26] Jüttner, K. (1990) Electrochemical Impedance Spectroscopy (EIS) of Corrosion Processes on Inhomogeneous Surfaces. *Electrochimica Acta*, **35**, 1501-1508. https://doi.org/10.1016/0013-4686(90)80004-8

[27] Jorcin, J.B., Orazem, M.E., Pebere, N. and Tribollet, B. (2006) CPE Analysis by Local Electrochemical Impedance Spectroscopy. *Electrochimica Acta*, **51**, 1473-1476. https://doi.org/10.1016/j.electacta.2005.02.128

[28] Shoar Abouzari, M.R., Berkemeier, F., Schmitz, G. and Wilmer, D. (2009) On the Physical Interpretation of Constant Phase Elements. *Solid State Ion*, **180**, 922-927. https://doi.org/10.1016/j.ssi.2009.04.002

[29] John, D.G., Searson, P.C. and Dawson, J.L. (1981) Use of AC Impedance Technique in Studies on Steel in Concrete in Immersed Conditions. *British Corrosion Journal*, **16**, 102-106. https://doi.org/10.1179/000705981798275002

[30] Berndt, L., Kleemeier, M., Thiel, K., Hartwig, A. and Burchardt, M. (2018) Anodization of Aluminum in Highly Viscous Phosphoric Acid PART 1: Investigation of Anodic Oxide Layers by Scanning Electron Microscopy (SEM) and *In-Situ* Electrochemical Impedance Spectroscopy (*in-Situ* EIS). *International Journal of Electrochemical Science*, **13**, 8867-8888. https://doi.org/10.20964/2018.09.11

[31] Deyab, M.A., Abd El-Rehim, S.S., Hassan, H.H. and Shaltot, A.M. (2020) Impact of Rare Earth Compounds on Corrosion of Aluminum Alloy (AA6061) in the Marine Water Environment. *Journal of Alloys and Compounds*, **820**, Article ID: 153428. https://doi.org/10.1016/j.jallcom.2019.153428

[32] Liu, C., Zhou, Z. and Li, K.Y. (2017) Improved Corrosion Resistance of CoCrMo Alloy with Self-Passivation Ability Facilitated by Carbon Ion Implantation. *Electrochimica Acta*, **241**, 331-340. https://doi.org/10.1016/j.electacta.2017.04.127

[33] Mishra, P., Yavas, D., Bastawros, A.F. and Hebert, K.R. (2020) Electrochemical Impedance Spectroscopy Analysis of Corrosion Product Layer Formation on Pipeline Steel. *Electrochimica Acta*, **346**, Article ID: 136232. https://doi.org/10.1016/j.electacta.2020.136232